Journal of Petroleum Science and Engineering 180 (2019) 456–470

Contents lists available at ScienceDirect

Journal of Petroleum Science and Engineering

journal homepage: www.elsevier.com/locate/petrol

A review of the phenomenon of counter-current spontaneous imbibition: Analysis and data interpretation

Abdul Salam Abd[a], Elsiddig Elhafyan[a], Abdul Rafey Siddiqui[a], Wajdi Alnoush[a], Martin J. Blunt[b], Nayef Alyafei[a,*]

[a] Department of Petroleum Engineering, Texas A&M University at Qatar, Doha, Qatar
[b] Qatar Carbonates and Carbon Storage Research Centre, Department of Earth Science and Engineering, Imperial College London, SW7 2AZ, United Kingdom

ARTICLE INFO

Keywords:
Spontaneous imbibition
Counter-current
Capillary dominated flow
Oil recovery
Semi-analytical solution
Numerical modelling
Capillary pressure
Relative permeability
Scaling of spontaneous imbibition
Boundary condition
Capillary back pressure

ABSTRACT

Spontaneous imbibition is an area of significant interest to the petroleum industry due to its large contribution to oil production in mature and fractured fields. This work discusses the physics behind the phenomenon of counter-current spontaneous imbibition: the key studies and experiments are reviewed along with how these projects influenced the understanding of the process. The work also simplifies the derivation of the semi-analytical solution of counter-current spontaneous imbibition (Schmid et al. 2011, 2016) and the equation by Schmid et al. (2012) to upscale the rate of spontaneous imbibition from the core to the field scales. Numerical applications of the solution for counter-current spontaneous imbibition, such as determination of relative permeability and capillary pressure, and oil recovery calculations are also discussed. The purpose of this work is to provide a clear and presentative overview of the main mathematical and theoretical concepts and their applications. The work compiles previous significant contributions to the topic and addresses development and applications of the semi-analytical solution, counter-current SI upscaling schemes, imbibition mechanisms and role of capillary backpressure.

1. Introduction

Understanding the phenomenon of spontaneous imbibition (SI) has become increasingly important due to the gradual transition of production from simpler, more homogeneous reservoirs, to highly fractured, dual porosity reservoirs, which currently make up most of today's global oil reserves (Saidi, 1983; Yu et al., 2009; Salimi and Bruining, 2010; Gong and Rosen, 2018). Spontaneous imbibition is defined as, "the process by which a wetting fluid is drawn into a porous medium by capillary action" (Morrow and Mason, 2001). This process only occurs when the wetting fluid displaces the non-wetting fluid out of the pore-space. This typically happens when the pore space is mostly saturated with the non-wetting fluid (the capillary pressure, $P_c = P_{nw} - P_w$, must be positive) (Anderson, 1986). Spontaneous imbibition occurs when the wetting phase, initially, rapidly occupies the more permeable regions of the pore space, such as fractures, followed by imbibition into the matrix, where most of the oil is contained (Fig. 1) (Kleppe and Morse, 1974; Gilman and Kazemi, 1983; Al-Hadhrami and Blunt, 2001).

The process of SI occurs in two ways depending on the direction of flow of the wetting and non-wetting phases. Co-current SI refers to when both the wetting and non-wetting phases move in the same direction, while counter-current SI is when the wetting and non-wetting phases move in opposite directions (Unsal et al., 2007a,b). There are two main differences in these processes: the first difference is that viscous coupling between the phases can mean that the relative permeability for co-current processes will be higher than counter-current flow (Bourbiaux and Kalaydjian, 1990). The second difference is that in counter-current flow, the non-wetting phase has to escape from the inlet through which the water imbibes in. Therefore, this can give rise to capillary backpressure when a finite capillary pressure is needed for the oil to be produced (Meng et al., 2017a, 2017b). These two processes are illustrated in Fig. 2.

This review will mainly focus on counter-current SI due to its significance in the process of fluid exchange between matrix and fractures during oil production via natural fractures (Qasem et al., 2008; Hatiboglu and Babadagli, 2008). Furthermore, even in large-scale geometries where co-current flow is possible, as illustrated in Fig. 2, there will always be some degree of counter-current flow, since the oil can always be displaced from the inlet; thus counter-current flow always dominates initially (Nooruddin and Blunt, 2016).

* Corresponding author.
E-mail address: nayef.alyafei@qatar.tamu.edu (N. Alyafei).

https://doi.org/10.1016/j.petrol.2019.05.066
Received 20 March 2019; Received in revised form 7 May 2019; Accepted 27 May 2019
Available online 31 May 2019

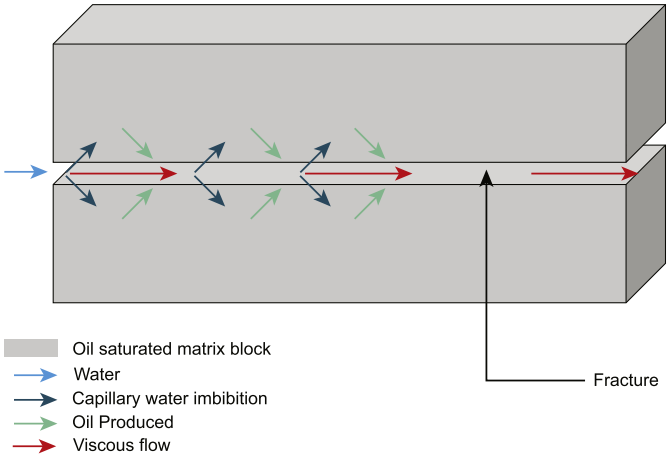

Fig. 1. An illustration of how spontaneous water imbibition can play an important factor in the production of oil in fractured reservoirs.

The objective of this work is to provide a central source describing previous key breakthroughs in the study of counter-current SI, to give a detailed explanation and derivation of the counter-current SI semi-analytical solution, and to model experiments for different boundary conditions and fluid exchange scenarios that should be taken into consideration when predicting fluid flow within oil reservoirs.

2. Theory and experiment

2.1. The discovery and foundations of spontaneous imbibition

The first proof of concept experiment for spontaneous imbibition was conducted and published by Washburn (1921) using a single capillary tube where water displaced air. Washburn (1921) provided an analytical solution for the movement of an air/water meniscus, assuming negligible viscosity of air, and demonstrated that the distance moved by the wetting phase scaled as the square root of time, confirming the findings of previous works (Bell and Cameron, 1906; Lucas, 1918). Subsequently, this analysis has been extended to consider fluids of finite viscosity (Morrow and Mason, 2001).

The derivation for spontaneous imbibition begins with defining the capillary pressure in an ideal capillary tube of fixed radius r, a perfectly wetting fluid and an interfacial tension with the invading fluid σ:

$$P_c = \frac{2\sigma}{r} \tag{1}$$

Assuming Laminar flow, the Poiseuille equation is used to describe laminar flow in a capillary tube. The mean velocity υ, is:

$$\upsilon = \frac{\Delta P}{x}\frac{r^2}{8\mu} \tag{2}$$

where μ is the fluid viscosity, and ΔP is the pressure drop across a length x. As stated, it is fair to assume that the flow during spontaneous imbibition is laminar, due to the slow nature of the process (Li et al., 2018). The value of x represents the length that the water has reached in the tube. The value of ΔP can be assumed to be constant, being the pressure difference between the inlet (P_{in}) and outlet (P_{out}). The capillary tube can also be assumed to be completely horizontal, nullifying the effect of gravity. The value of ΔP hence must remain positive, with flow remaining in the direction of inlet to outlet, and $\Delta P = P_{in} - P_{out}$ (Blunt, 2017).

If assumed that the invading fluid is of negligible viscosity (i.e. gas), the main driving force for fluid flow would be capillary pressure, P_c and the viscous resistance is proportional to the invaded length. Substituting Equation (1) in Equation (2) yields the following expression (Morrow and Mason, 2001):

$$\upsilon = \frac{2\sigma}{r}\frac{1}{x}\frac{r^2}{8\mu} = \frac{\sigma r}{4\mu x} \tag{3}$$

Since velocity $\upsilon = dx/dt$, the equation can be integrated to find:

$$x^2 = \frac{\sigma r t}{2\mu} \tag{4}$$

Equation (4) is easily generalized for the case where the displaced fluid has a finite viscosity, μ_d, and a viscosity ratio M is defined as $M = \mu_d/\mu$ (Morrow and Mason, 2001; Blunt, 2017):

$$(1 - M)x^2 + 2MLx = \frac{\sigma r t}{2\mu} \tag{5}$$

where L is the total length of the tube.

The main result is that when the flow is limited by the invading wetting phase flow, the distance travelled scales as the square root of time; this will be used later when the semi-analytical solution for spontaneous imbibition is derived.

2.2. Analysis of connected capillary tubes

While the treatment of flow in a single capillary is instructive, a porous medium can be thought of having many interconnected capillaries of different sizes. Hence, extensions from the one-tube case are necessary to understand more realistic flows. Dong et al. (1998) considered two parallel tubes with a porous interaction boundary between them (Fig. 3). The tubes had different radii with connections between them, so that the same fluid phase at the same distance from the inlet would have the same pressure.

The situation shown in Fig. 3 consists of three main regions that represent different flow and pressure characteristics. In region (l_1) water occupied both tubes, and therefore the water pressure in the tubes at the same distance x was the same. A similar statement can be made for region (l_3) where oil occupied both capillaries and therefore a unified phase pressure for both capillary tubes is observed. The difference occurs in region (l_2) where at the meniscus in tube 1 there is a pressure difference between the phases, P_{c1}. There are different pressure gradients in the water and oil phases in the two phases to accommodate a larger capillary P_{c2} at the second meniscus. This analysis shows that the wetting phase advances faster through the smaller capillary, since it has the greater capillary pressure driving imbibition. The connectivity of the pore network is crucial for this to occur: based simply on the Washburn (1921) analysis, imbibition is faster in a larger radius capillary, since the flow resistance is lower. However, in a connected network, the wetting phase experiences the same pressure gradients regardless of the local radius of the pore.

Several authors have extended this work by Dong et al. (1998) to analyze imbibition in interconnected capillary tubes, again confirming that advance is faster in the smaller radius pores (Dong and Dullien, 1997; Bartley and Ruth, 1999; Ruth and Bartley, 2011). This arrangement of capillary tubes approximates scenarios similar to those observed in porous media. Typically, those would contain capillary throats that allow cross-flow. Therefore, it must be taken into consideration when predicting spontaneous imbibition at the field scale.

The previous analysis has been for co-current flow: in counter-current flow, on the other hand, the non-wetting phase has to escape back through the inlet. The works of Unsal et al. (2007a, 2007b, 2009) were the first to study, both experimentally and analytically, imbibition with asymmetrical geometries. Counter-current imbibition was only possible if the non-wetting phase had a finite backpressure to allow it to be produced through the inlet. These experiments were performed by placing a rod against a glass plate with flow barriers placed on either side of the rod and sealing against the glass plate. Adjusting the space between the rod and the glass plate laterally, allowed the gap through which the non-wetting phase had to escape to be altered, hence changing the capillary backpressure, as illustrated in Fig. 4.

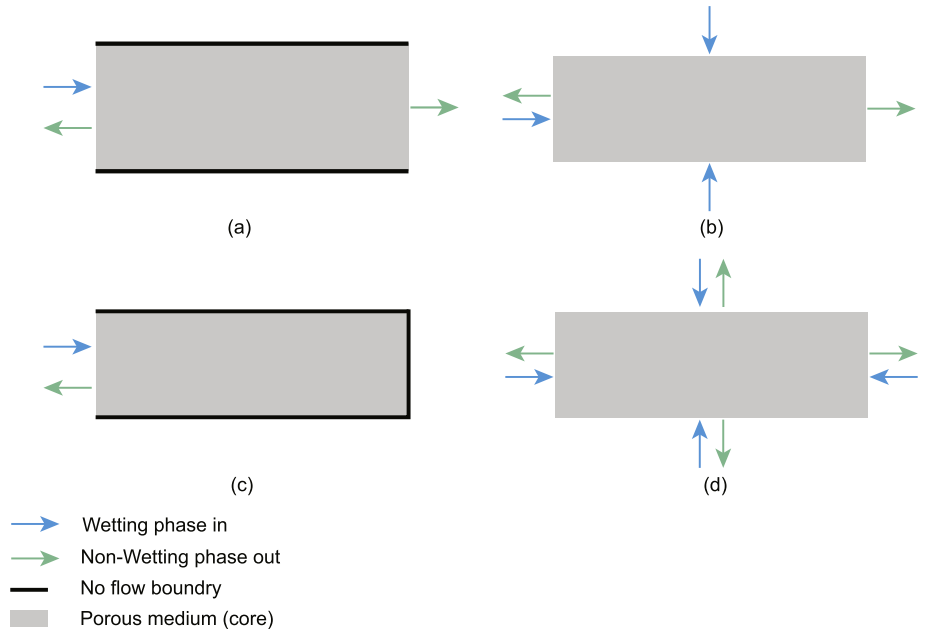

Fig. 2. Different imbibition scenarios. (a) and (b) display geometries where there is a combination of counter- and co-current spontaneous imbibition. (c) and (d) show counter-current spontaneous imbibition. Reproduced from Mirzaei-Paiaman et al. (2017).

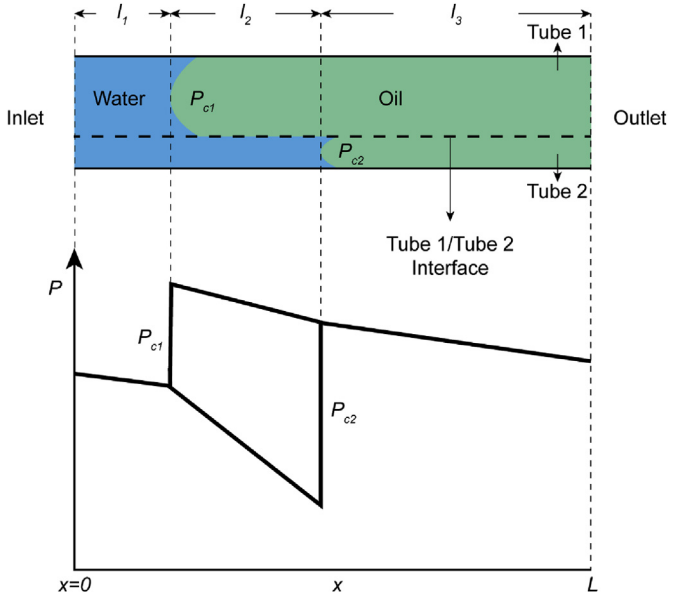

Fig. 3. Schematic showing displacement of oil using water in two interconnected capillary tubes (connected via the dotted line) with the corresponding plot of phase pressure with x = 0 being the inlet and x = L being the outlet. The effect of capillary pressure at the menisci is illustrated. This analysis explains why, in a connected pore network, the wetting phase advances faster in tubes of smaller radius. Reproduced from Dong et al. (2005).

Unsal et al. (2009) showed that if counter-current flow was prevented and imbibition occurred through non-interacting capillaries, then the wetting phase moved faster in the larger radius pores. However, if the non-wetting phase was allowed to escape through the inlet, through the formation of bubbles with a finite backpressure, then imbibition could proceed more rapidly through the smaller capillaries.

The work of Unsal et al. (2009) is significant because it investigated spontaneous imbibition in non-circular capillaries unlike most preceding works. It also investigated the shape of the imbibition shock front concluding that imbibition has similarities to Buckley-Leverett analysis. In their model, they related the rate of counter-current imbibition to the dead-end pressure P_{dead} created at the interface between the two capillaries. As the distance d between the rod and glass plate varies, the value of P_{dead} changes. These changes lead to changes in the rate of counter-current imbibition relative to co-current imbibition. Due to irregularities in the shape of the capillaries and the presence of both co- and counter-current flow with an inlet, which occasionally allows air bubbles to enter, a model to represent imbibition for such scenario was created. However, an analytical solution was not found due to associated complexities (Unsal et al., 2007a,b). This experiment along with other experiments of bundled capillary tubes showed the necessity to find analytical solutions which can accommodate the complex structure of natural porous media.

2.3. Semi-analytical solution for counter-current SI

While simple analyses of spontaneous imbibition in capillary tubes are interesting, a more general approach to the problem of SI requires solutions using averaged continuum equations for flow in porous media. Several authors have provided analytical solutions for SI, but only for rather restrictive and often unrealistic functional forms for the capillary pressure and relative permeabilities (Fokas and Yortsos, 1982; Kashchiev and Firoozabadi, 2003). Several developments of an analytical solution to predict capillary flow were published. McWhorter and Sunada (1990, 1992) proposed a general semi-analytical solution for SI, but it was largely ignored in the literature since it appeared to assume a rather specific form of the inlet boundary condition. Schmid et al. (2011) revisited this solution and showed that it in fact was a general solution applicable for counter-current flow. Later work presented further solutions and various methods to construct saturation profiles and recoveries (Bjørnarå and Mathias, 2013). Next, systematic analysis and suggestions on how to calculate solutions to the governing equations for flow are discussed.

First, one-dimensional counter-current flow of two immiscible, incompressible phases through a homogeneous porous medium is considered. In counter-current flow, the water invades a closed system and oil leaves in the opposite direction. The derivation of the analytical solution for this counter-current SI will be explained in the following steps based on the study of Schmid et al. (2011, 2016). The semi-analytical solution is developed based on the following assumptions:

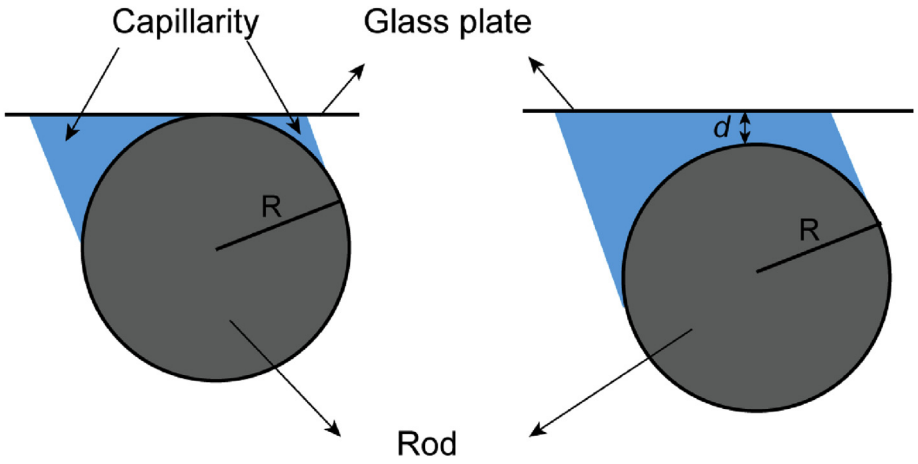

Fig. 4. A schematic of the experimental arrangement to test counter-current imbibition. Reproduced from Unsal et al. (2009).

1. Gravitational forces are neglected.
2. The system is homogeneous.
3. The fluids are incompressible.
4. The inlet capillary pressure is zero with no capillary backpressure.
5. The traditional multi-phase Darcy law is applicable for this process.
6. The solutions are a function of the parameter $\omega = x/\sqrt{t}$ for early time, before the imbibing water front reaches the far boundaries of the sample. This, is however, the general case for counter-current SI.

The one-dimensional conservation of mass equation for incompressible fluids can be expressed as:

$$\phi\frac{\partial S_w}{\partial t} + \frac{\partial q_w}{\partial x} = 0 \tag{6}$$

where ϕ is the porosity, S_w is the water saturation, q_w is the water velocity, t is time and x is distance.

The wetting phase Darcy velocity equation (Dake, 1983; Helmig, 1997) can be written as:

$$q_w = \frac{\lambda_w}{\lambda_t}\left[q_t + k\lambda_{nw}\left(\frac{\partial P_c}{\partial x} + (\rho_w - \rho_{nw})g_x\right)\right] \tag{7}$$

where λ_w is the mobility of the wetting phase (water), λ_{nw} is the mobility of the non-wetting phase (oil), λ_t is the total mobility, q_t is the total velocity of the wetting and non-wetting phase, k is the absolute permeability, p_c is the capillary pressure defined as the difference between the non-wetting and wetting phase pressures, ρ_w is the density of the wetting phase, ρ_{nw} is the density of the non-wetting phase and g_x is the gravitational acceleration in the flow direction.

Ignoring gravitational forces, yields:

$$q_w = \frac{\lambda_w}{\lambda_t}q_t + \frac{k\lambda_w\lambda_{nw}}{\lambda_t}\left(\frac{\partial P_c}{\partial x}\right) \tag{8}$$

The Buckley-Leverett fractional flow is defined as $f_w = \frac{\lambda_w}{\lambda_t}$, and the equation becomes:

$$q_w = f_w q_t + \frac{k\lambda_w\lambda_{nw}}{\lambda_t}\left(\frac{\partial P_c}{\partial x}\right) \tag{9}$$

Differentiating the wetting phase velocity with respect to x, gives:

$$\frac{\partial q_w}{\partial x} = \frac{\partial}{\partial x}\left(\frac{k\lambda_w\lambda_{nw}}{\lambda_t}\left(\frac{\partial P_c}{\partial x}\right)\right) \tag{10}$$

Next, Equation (10) is substituted in the conservation expression, Equation (6), to give:

$$\phi\frac{\partial S_w}{\partial t} + \frac{\partial}{\partial x}\left[\frac{k\lambda_w\lambda_{nw}}{\lambda_t}\left(\frac{\partial P_c}{\partial x}\right)\right] = 0 \tag{11}$$

Now, according to Barenblatt et al. (1990, 2003), the capillary dispersion coefficient can be defined as:

$$D(S_w) = -\frac{k\lambda_w\lambda_{nw}}{\lambda_t}\frac{dP_c}{dS_w} \tag{12}$$

When this coefficient is substituted into Equation (11):

$$\phi\frac{\partial S_w}{\partial t} = \frac{\partial}{\partial x}\left[D(S_w)\frac{\partial S_w}{\partial x}\right] \tag{13}$$

In the traditional Buckley-Leverett analysis (ignoring capillary forces), the solution of this flow equation is a function of $v = \frac{x}{t}$, where v is the dimensionless wave speed. Alternatively, with capillary-controlled flow, it is proposed that the distance x, representing the imbibing front, scales with $\sqrt{t}$ instead of t (Handy, 1960; Babadagli and Ershaghi, 1992; Garg et al., 1996; Li and Horne, 2000; Olafuyi et al., 2007; Alyafei et al., 2014; Alyafei and Blunt, 2018). Hence, the attempt to find the flow equation is pursued by defining the scaling factor ω as:

$$\omega = \frac{x}{\sqrt{t}} \tag{14}$$

The scaling used is only valid under the assumptions listed earlier, and specifically when the flow is entirely driven by capillary forces within the rock.

The following derivatives are defined:

$$\frac{\partial S_w}{\partial t} = \frac{dS_w}{d\omega}\frac{\partial \omega}{\partial t} = -\frac{\omega}{2t}\frac{dS_w}{d\omega} \tag{15}$$

$$\frac{\partial S_w}{\partial x} = \frac{dS_w}{d\omega}\frac{\partial \omega}{\partial x} = \frac{1}{\sqrt{t}}\frac{dS_w}{d\omega} \tag{16}$$

Substituting Equations (15) and (16) into the counter-current flow Equation (13), yields:

$$\omega\frac{dS_w}{d\omega} = -\frac{2}{\phi}\frac{d}{d\omega}\left[D(S_w)\frac{dS_w}{d\omega}\right] \tag{17}$$

Equation (17) is then integrated:

$$\int \omega.\, dS_w = -\frac{2D}{\phi}\left(\frac{dS_w}{d\omega}\right) \tag{18}$$

Then, from analogy with the Buckley–Leverett analysis, for some capillary fractional flow F ($1 \geq F \geq 0$) and constant C, ω can also be defined as:

$$\omega = \frac{2CF'}{\phi} \tag{19}$$

Here, the factor $2C/\phi$, where C is a constant, is introduced to make F dimensionless. Differentiating ω with respect to S_w gives:

$$\frac{d\omega}{dS_w} = \frac{2CF''}{\phi} \tag{20}$$

Substituting Equations (19) and (20) into Equation (18) and integrating gives:

$$\frac{2CF}{\phi} = -\frac{D}{CF''} \tag{21}$$

Through rearranging:

$$FF'' = -\frac{\phi}{2C^2}D \tag{22}$$

Equation (22) is an implicit non-linear second-order ordinary differential equation. Unlike a full numerical solution to the governing partial differential equations in both space and time, Equation (22) can be solved simply, as will be illustrated below. The key difference between this development and the waterflood Buckley-Leverett problem, is that the total amount of fluid that enters the system is no longer boundary condition, rather it is now embedded in the constant C. This necessitates an iterative solution, which makes numerical solutions to Equation (8) so problematic. As an initial error in the imbibition rate propagates, it yields very poor numerical solutions, unless a grid that is unfeasibly refined in both space and time is used (Nooruddin and Blunt, 2016). Instead, Equation (22) is discretized in saturation space, which, as shown, is a very quick and accurate method to find a solution.

The backward difference method will be used to discretize Equation (22) (Canale and Chapra, 1998). An initial value of C is estimated knowing that $F(S_w^*) = 1$ and $F'(S_w^*) = 0$. This sets the initial conditions to calculate F for lower values of saturation. A converged solution is found when $F(S_{wir}) = 0$.

F' and F'' are defined in the following way:

$$F'(S_i) = \frac{F(S_i) - F(S_{i-1})}{\Delta s} \tag{23}$$

$$F''(S_i) = \frac{F(S_{i-2}) - 2F(S_{i-1}) + F(S_i)}{\Delta s^2} \tag{24}$$

The following substitution will also be used to obtain an equation in terms of x:

$$F(S_i) = X \tag{25}$$

Substituting Equations (23)–(25) into Equation (22) yields:

$$X^2 + X[F(S_{i-2}) - 2F(S_{i-1})] + \frac{\phi}{2C^2}D\Delta s^2 = 0 \tag{26}$$

The above follows the quadratic equation of the form $ax^2 + bx + c = 0$, with the coefficients a, b and c being defined as:

$$a = 1 \tag{27}$$

$$b = F(S_{i-2}) - 2F(S_{i-1}) \tag{28}$$

$$c = \frac{\phi}{2C^2}D\Delta s^2 \tag{29}$$

Using the quadratic formula, the following solution for the counter-current flow equation is achieved:

$$X = F(S_i) = \frac{-b \pm \sqrt{b^2 - 4ac}}{2a} \tag{30}$$

$$F(S_i) = \frac{-[F(S_{i-2}) - 2F(S_{i-1})] + \sqrt{[F(S_{i-2}) - 2F(S_{i-1})]^2 - 4\left(\frac{\phi}{2C^2}D\Delta s^2\right)}}{2} \tag{31}$$

$$F(S_i) = [F(S_{i-1}) - 0.5F(S_{i-2})] + \sqrt{[0.5F(S_{i-2}) - F(S_{i-1})]^2 - \frac{\phi}{2C^2}D\Delta s^2} \tag{32}$$

To solve for C and F, one would have to solve the integral implicitly. However, a simple spreadsheet program utilizing the concept of backward-differencing approximation through an iterative process to find the unknown constant C is used (Schmid et al., 2016; Alyafei et al., 2016). This spreadsheet makes use of the following equations:

$$F(S_{wir}) = 0 \tag{33}$$

$$\sum_{i=1}^{n} F'(S_w, i)\,.\,\Delta S_w \approx F(S_w^*) = \frac{Q_w(t)}{\phi} = \frac{\phi}{2C\sqrt{t}} = 1 \tag{34}$$

The solution process is as follows:

1 Determine F“ from a backward-differencing approximation.
2 Iteratively determine (S_w) at a finite number n of saturation points.
3 Iterate on the constant C until $F(S_w)$ converges to the correct solution.

The final value of C is obtained when Equation (33) converges to 0, and Equation (34) converges to 1. Example solutions are shown in later sections of this paper. Convergence on C to 4 significant figures is typically obtained within 4 iterations.

Moreover, the semi-analytical solution can be used to derive the upscaling group of Schmid and Geiger (2012, 2013) through simple manipulation of the variables. This scaling group is based on the frontal movement of the wetting phase:

$$t_{D,front} = \left(\frac{x_{front}(t)}{\phi L_c}\right)^2 = \left(\frac{2C}{\phi L_c}F'(S_{wir})\right)^2 \tag{35}$$

The dimensionless time can be further interpreted as:

$$q_w(t) = 2C\sqrt{t} \tag{36}$$

Hence, the dimensionless time becomes:

$$t_D = \left(\frac{q_w(t)}{\phi L_c}\right)^2 \tag{37}$$

where L_c is the characteristic length to account for the variation in the profile of the fluid saturation. A deeper analysis on the role of the characteristic length will be presented in the upscaling section of the paper.

2.4. Imbibition mechanisms for different boundary conditions

So far, only a one-dimensional analysis has been presented, while real reservoir geometries are three-dimensional. To bridge this gap in our understanding, several studies have been conducted with different boundary condition scenarios in a two-dimensional plane (Morrow and Mason, 2001; Mason et al., 2009; Arabjamaloei and Shadizadeh, 2010; Nooruddin and Blunt, 2016; Khan et al., 2018). Even though all these scenarios can apply in reservoir situations, it is still very difficult to predict the impact of each to counter-current SI. The four main boundary conditions are displayed in Fig. 5 (Morrow and Mason, 2001) and are named:

a) All Faces Open (AFO): The wetting phase flows into and out of the core from all sides.
b) One End Open (OEO): The wetting phase flows into the core from one side horizontally with the rest sides of the core are sealed.
c) Two Ends Open (TEO): The wetting phase flows axially from end to end in the core, while the top and bottom sides are sealed.
d) Two Ends Closed (TEC): The wetting phase flows in a vertical line from top to bottom, while the other sides are completely isolated.

To test the phenomenon of counter-current SI, much dependence still lies on the two main scenarios of OEO and TEO (Ruth and Arthur, 2011).

Regardless of the boundary condition imposed on the core, the

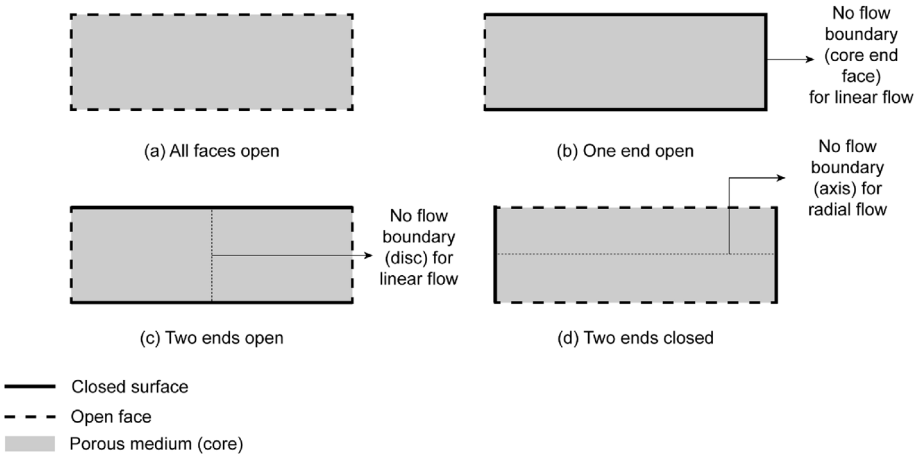

Fig. 5. Schematic showing (a) All Faces Open (AFO), (b) One End Open (OEO), (c) Two Ends Open (TEO), and (d) Two Ends Closed (TEC).

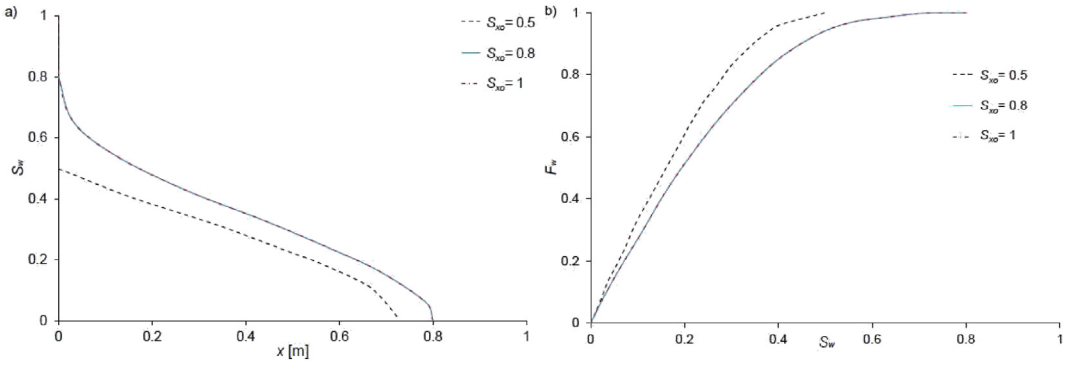

Fig. 6. (a) A plot of water saturation as a function of distance from the water inlet. The saturation value at the inlet, which is affected by the capillary backpressure, has an effect on how the water saturation changes with space. (b) A plot of the capillary fractional flow for different inlet saturations. Reproduced from Foley et al. (2017).

sample should be adequately represented with a suitable shape factor. The shape factor is mainly used to account for the variations in the boundary condition for SI systems as a correction to compute the effective imbibition rate. The equation for the shape factor was developed by Kazemi et al. (1992):

$$F_s = \frac{1}{V_b}\sum_{i=1}^{j}\frac{A_i}{\delta_{A_i}} \tag{38}$$

where V_b is the bulk volume of the matrix block, A_i is the surface area open to imbibition in the i-th direction, $\delta_{A_i}$is the distance from the open surface to the center of the matrix block, and j is the total number of surfaces open to the imbibition.

The inverse of the square root of the shape factor is the characteristic length L_s. Based on this parameter, Ma et al. (1997) proposed a modified characteristic length:

$$L_c = \sqrt{\frac{V_b}{\sum_{i=1}^{n}\frac{A_i}{l_{A_i}}}} \tag{39}$$

where A_i is the distance travelled by the imbibition front the open surface to the to the non-flow boundary.

The characteristic length can be then integrated into the dimensionless time of SI, along with the volume of water imbibed from the inlet into the rock sample which is used to predict the recovery factors for each boundary condition.

In all cases, the behavior can be approximated by a semi-analytical solution and a dimensionless time given by Equation (37) but where the term $1/L_c^2$ is replaced by the shape factor F_s. With an appropriate choice of shape factor, the quantitative behavior of imbibition can be found even in more complex two- and three-dimensional geometries.

2.5. Role of capillary backpressure

The capillary backpressure is defined as the pressure that the oil phase needs to overcome, to be produced counter-currently (Haugen et al., 2014; Andersen et al., 2017; Foley et al., 2017). The ingress of water has to be matched by the displacement of oil, and this may limit the imbibition rate, particularly for tight rocks, with high capillary pressures or for viscous oils. The backpressure is, physically, likely to be equal, or close to, the capillary entry pressure for the non-wetting phase in drainage.

If there is a threshold or capillary backpressure, P_{cb}, at the inlet, then the inlet saturation S_i is found such that $P_c\ (S_i) = P_{cb}$. The semi-analytical solution can be used as described in the previous section, but with a different inlet boundary condition. It has been shown that for most water-wet systems, reasonable estimates of the likely backpressure do not significantly affect the saturation profile or overall imbibition rate, since the water saturation tends to drop sharply with distance near the inlet (Foley et al., 2017). As shown in Fig. 6, significant effects are only observed if the capillary backpressure is very large and results in a much lower inlet saturation than for $P_c = 0$.

3. Numerical analysis of counter-current SI

3.1. Model description

In this section, a review is presented on the main guidelines available in the literature that aid the reader in understanding approaches to

modelling counter-current spontaneous imbibition without using specialized core simulators.

Khan et al. (2018) simulated SI using a fully implicit general-purpose black oil reservoir simulator. The grid was based on a corner point approach employing a classical finite-difference scheme while the flow equations were based on the conservation of mass and Darcy flow. Three wettability cases were used to model counter-current SI; strongly water-wet (SWW), weakly water-wet (WWW) and mixed-wet (MW). The power-law model was used for relative permeabilities and capillary pressures where the exponents are based on the data provided by Schmid et al. (2016) and Blunt (2017).

$$k_{rw} = k_{rw,max}\left(\frac{S_w - S_{wi}}{1 - S_{wir} - S_{or}}\right)^n \tag{40}$$

where k_{rw} is the water relative permeability, $k_{rw,max}$ is the maximum water relative permeability, S_w is the water saturation S_{wi} is the initial water saturation, S_{gr} is the residual gas saturation, and n is the Corey water exponent.

$$k_{ro} = k_{ro,max}\left(\frac{1 - S_w - S_{wi}}{1 - S_{wir} - S_{or}}\right)^m \tag{41}$$

where k_{ro} is the oil relative permeability, $k_{ro,max}$ is the maximum oil relative permeability, and m is the Corey oil exponent.

$$P_C = P_{c,entry}\left(\frac{S_w - S_{wi}}{1 - S_{wi} - S_{or}}\right)^l \tag{42}$$

where P_C is the capillary pressure, $P_{c,entry}$ is the entry capillary pressure and l is the capillary pressure exponent.

The exponent l corresponding to the capillary pressure curve in Schmid et al. (2016) data was modified from the original study and was set to be the same for all the wettability cases. To demonstrate the effect of wettability, the value of S_w* at which the capillary pressure becomes zero, and the spontaneous imbibition process stops, was varied. Beyond this point, any further recovery would require forced displacement through water injection. The value of S_w* for mixed-wet cases was expected to be much lower compared to the strongly water-wet exemplar, since some fraction of the pore space will be oil-wet and cannot be recovered by spontaneous imbibition of water. The exponents n and m for the relative permeability relationships control the shape of the oil and water curve respectively.

The data in Table 1 and Table 2 summarize the parameters used to construct the relative permeability and capillary pressure for the discussed cases, while Fig. 7 shows the relative permeabilities and capillary pressures for the different wetting states.

In the work of Khan et al. (2018), it was assumed that the rock properties such as porosity and permeability were constant. The main grid was a 1-D Cartesian lattice with 400 cells varying in the i-th direction, and only two phases are modelled at a time. The grid describes a conventional core sample of a sandstone rock represented as a rectangular prism. Moreover, the change in the saturation of the flowing phases along with their respective pressure is calculated in each cell at each time step. The main body of the core is attached to a cell that acts as a water tank characterized with high permeability and porosity. The water flows spontaneously from the water tank into the core, while the oil flows in the opposite direction from the core onto the water tank. The purpose of the simulator is to quantify the saturation of the water phase along the distance of the simulated core. The SI modelling process is explained in further detail are in Khan et al. (2018) and Abd and Alyafei (2018).

Table 1
Saturation function parameters used in the analytical solution for the cases used in this study based on Schmid et al. (2016).

Parameter	SWW	MW
S_{wir}	0.2	0.2
S_{or}	0.4	0.1
$k_{rw\ max}$	0.2	0.6
n	3	3
$k_{ro\ max}$	0.85	0.8
m	1.5	8
P_{entry} [kPa]	12	12
l	−0.7	−0.2
μ_w [$mPa.\ s$]	1	1
μ_o [$mPa.\ s$]	3	1
C [$m/\sqrt{s}$]	4.63×10^{-5}	2.75×10^{-5}

Table 2
Saturation function parameters used in the analytical solution for the cases used in this study based on Blunt (2017) and used by Khan et al. (2018).

Parameters		SWW	WWW	MW
S_{wir}		0.1	0.1	0.1
S_{or}		0.4	0.3	0.15
S_w^*		0.6	0.6	0.5
$k_{rw\ max}$		0.1	0.2	0.5
n		2	2	8
$k_{ro\ max}$		1	1	1
m		1	1.5	2.5
P_{entry} [kPa]		200	100	100
l		0.3	0.3	0.3
C [m/√s]	M = 0.05	4.05×10^{-4}	3.40×10^{-4}	2.72×10^{-5}
	M = 1	3.46×10^{-4}	2.87×10^{-4}	2.64×10^{-5}
	M = 20	1.97×10^{-4}	1.48×10^{-4}	2.48×10^{-5}
	M = 200	8.92×10^{-5}	6.36×10^{-5}	1.76×10^{-5}

Earlier discussions entailed possible semi-analytical solutions. However, this section switches focus into numerical modelling of SI due to its importance in providing substantial information on the effect of key engineering parameters on reservoir performance; it can also be extended to relax some of the assumptions made in the analytical analysis, namely the consideration of both counter-current and co-current flows, compressible fluids and multi-dimensional flow geometries. The semi-analytical solutions will be used to understand the mechanism and the physical context of SI processes, and as a point of validation for the numerical solutions.

3.2. Saturation profiles

To study the effects of viscosity ratio and wettability on the saturation profiles, multiple simulations were run with in the data show in Tables 1 and 2 The results from Blunt (2017), who provided analytical solutions for these cases, showed a precise match for the numerical and the semi-analytical solutions regardless of the wide range of viscosity ratios. Moreover, the wettability of the rock did not have any noticeable effect on the quality of the match. It is noticed from the profiles in Fig. 8(a–c) that the water needs less time to fully saturate the rock at low viscosity ratios when the mobility of the oil is high. This observation is valid for all wetting states tested. However, it should be noted that different grid resolutions were used in each case. To achieve accurate simulation results and an acceptable match, 0.25% of the core volume has to be captured in each grid cell (Khan et al., 2018). The work of Khan et al. (2018) presents further analysis of the numerical results for different SI flow modes.

Further simulations were run using the Schmid et al. (2016) data set for two wettability cases and three viscosity ratios. In the first case, a core fully saturated with air was imbibed with water, and the water saturation profiles were plotted at five times. It was observed that the water front progresses steadily as time increases, and the five water saturation profiles scale perfectly with square root of time in both water-wet and mixed-wet cases. The profiles before and after scaling the saturation profiles can be seen in Fig. 9(a–b) for the SWW case.

The same procedure was repeated while changing the non-wetting phase to oil and testing different oil viscosities [1 mPa s and 3 mPa s]

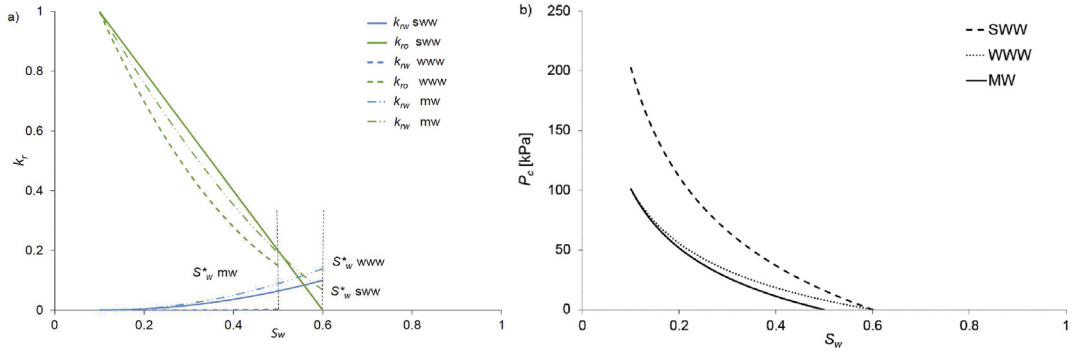

Fig. 7. (a) Relative permeabilities for the strongly water-wet SWW, weakly water-wet WWW and mixed-wet MW cases, as well as (b) the respective capillary pressures based on Blunt (2017). All the curves stop at their respective S_w^*. Reproduced from Khan et al. (2018).

with the water viscosity kept at a constant value of 1 mPa s. Results are reported with *M* representing the mobility ratio where the oil viscosity is divided by the water viscosity. Again, the same behavior is observed, as the profiles collapse onto one curve as a function of $x/\sqrt{t}$ as illustrated in Fig. 10(a–h), for any viscosity or wettability state. It is also noticed that the shape of the curves differs slightly between water-wet and mixed-wet cases when oil is used, as opposed to overlapping profiles in the gaseous state. The water profiles move slower when the rock is mixed-wet. In these situations, the ultimate recovery is expected to be much lower, and the imbibition rate may be several orders of magnitudes lower than water-wet cases. Theoretically, in a mixed wet-system, the process of spontaneous imbibition is limited to the zones where water saturation is small. The imbibition rate is limited by the water relative permeability at low water saturation which may be very small in mixed-wet systems (Blunt, 2017; Behbahani and Blunt, 2005; Behbahani et al., 2006).

3.3. Upscaling of counter-current SI

Extensive research has been done in the past to understand the phenomenon of spontaneous imbibition in water-wet rocks and to convert core-scale experimental data of oil recovery to the field-scale (Iffly et al., 1972; Prey and Lefebvre, 1978; Hamon and Vidal, 1986; Bourbiaux and Kalaydjian, 1990; Cuiec et al., 1994; Zhang et al., 1996; Cil et al., 1998; Rangel-German and Kovscek, 2002). Scaling transfer functions are used to predict recovery at the field scale using the results from lab experiments. However, information loss on upscaling is inevitable, thus brining attention to a key issue of how to optimize the upscaling techniques and minimize this information loss. A solid understanding of the flow functions governing fluid flow in fractured reservoirs provides the necessary foundation for upscaling laboratory results to the field scale using numerical simulators.

It is estimated that naturally fractured reservoirs contribute to around 50% of the hydrocarbon reserves discovered worldwide (Schlumberger, 2013). In such reservoirs, oil recovery is vastly improved when the appropriate recovery techniques are applied such as waterflooding (Muggeridge et al., 2014). Moreover, these reservoirs are usually represented as dual porosity simulation models. This is because the porosity differs vastly between the matrix of the rock and the fracture itself, and so does the permeability (Warren and Root, 1963). Moreover, the irregular shape of the network of fractures is characterized by high permeability and porosity creating a heterogeneous medium in the reservoirs that permits more fluid to flow to the surface.

Naturally fractured reservoirs are usually very difficult to characterize making predictions of recovery uncertain (Gilman and Kazemi, 1983). Since the fractures act as a conduit for the fluid flow, their properties control the behavior, yet they are difficult to characterize accurately (Thomas et al., 1983). As the hydrocarbons flow from the low-permeability matrix rock into the fracture conduit, spontaneous imbibition dominates. Specifically, the oil stored in the pores of the matrix is mobilized by the means of capillary pressure or gravity (Gilman and Kazemi, 1983). The illustration in Fig. 11 shows a fracture channel surrounded by the tight matrix block. Capillary forces push the oil from the pores of the rock into the flowing fracture carrying the hydrocarbon to the producer by the mean of water flooding. This variation in the saturation profile and the effect of the spontaneous imbibition process can be seen in the associated plot. This is more complex than the one-dimensional profiles shown previously, as the water penetrates into the matrix block dependent on the length of time that water has been present in the fracture.

The fluid communication between the matrix and the fracture block is modelled by a transfer function *T*. The first transfer function that accurately simulated dual behavior was developed by Barenblatt et al. (1960) using a continuum method approach. Transfer functions then adapted in the oil gas and industry by Warren and Root (1963):

$$T = \sigma \frac{k}{\mu}(P_m - P_f) \tag{43}$$

where, *T* is the transfer function [1/sec], σ is the shape factor $[1/m^2]$, *k* is the matrix permeability [m^2 or mD], μ is the viscosity [Pa.s], and P is

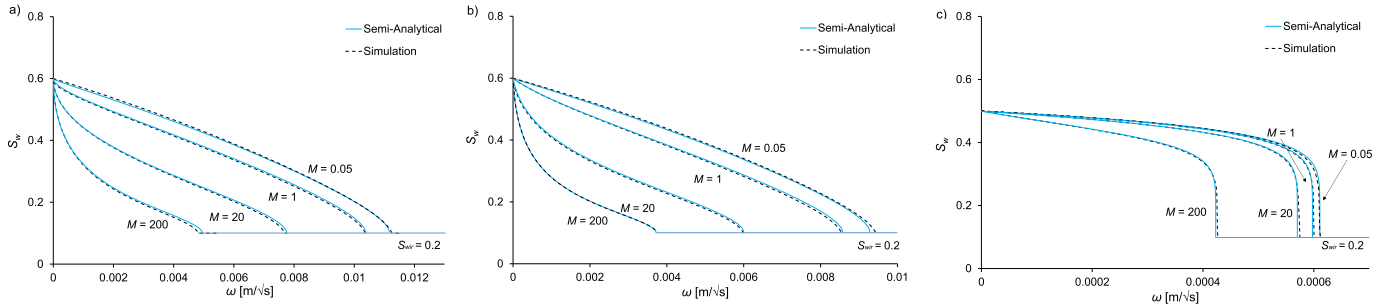

Fig. 8. A comparison between semi-analytical and numerical water saturation profiles for counter-current SI with varying mobility ratio, M, for (a) strongly water-wet case, (b) weakly water-wet case, and (c) mixed-wet case. Reproduced from Khan et al. (2018).

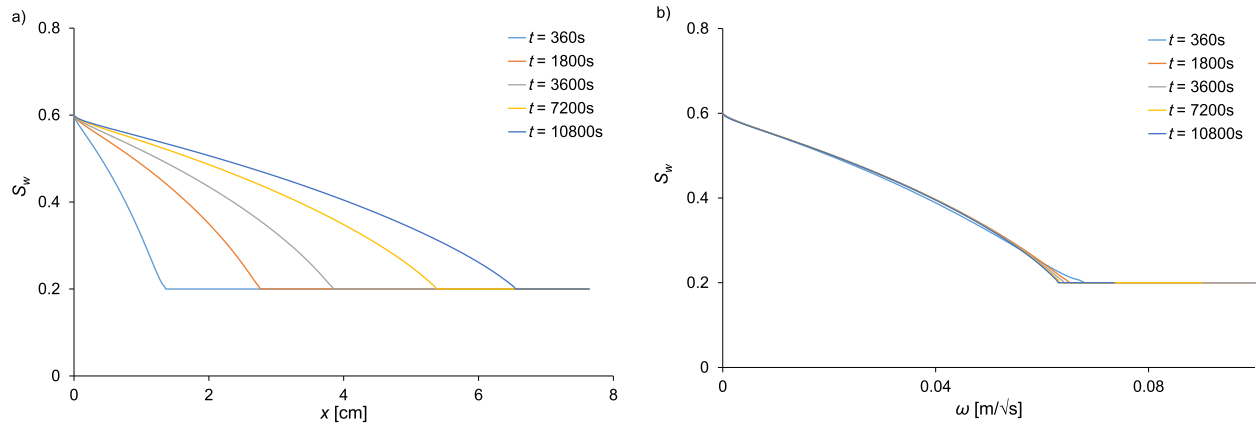

Fig. 9. Schematic showing (a) a comparison between semi-analytical water saturation profiles (air-water) for countercurrent SI at different times (b) the profiles progress with the distance as $\sqrt{t}$.

the pressure [Pa]; *m* and *f* stand for matrix and fracture respectively.

This model was subsequently further enhanced by Quandalle and Sabathier (1989), Gilman and Kazemi (1983), and Kazemi et al. (1976) to account for gravity, changes in water saturation and viscous recovery. Moreover, Chen et al. (1995) tweaked the transfer function to account for counter-current imbibition processes, and to model early and late time in water saturation profiles. Later on, a generalized transfer function was developed by Lu and Blunt (2007) to model capillary imbibition under mixed-wet conditions. Experimentally, the properties of fracture/matrix transfer functions have been the focus of many studies (Handy, 1960; Cil and Reis, 1996; Reis and Cil, 1999; Akin et al., 2000; Li and Horne, 2000; Rangel-German and Kovscek, 2002; Zhou et al., 2002; Abushaikha and Gosselin, 2008). The wetting fluid imbibition patterns and the rate of water flow in the fracture are obtained through lab measurements. Under lab conditions, the fractures are assumed to be "instantly-filled" with water, and CT-scanning techniques can be used to monitor the water frontal movement. The most common type of apparatus used for these experiments in visualized in Fig. 12.

The images collected through the CT-scanning technique allows us to calculate the average water saturation in the core as time progresses and relate it to the mass of the imbibed water linearly. This data permits the development and incorporation of scaling groups to find a shape factor for dual porosity simulation models.

The first attempt to scale oil recovery with dimensionless time was by Mattax and Kyte (1962) based on the work of Rapoport (1955). However, this scaling law was very restrictive as many rock and fluid properties needed to be considered to obtain an acceptable fit to the data. Although this scaling law was a big step in understating the behavior of naturally fractured water driven reservoirs, the effects of the geometry of the core, relative permeability, viscosity ratios, gravity forces and capillary pressure need to be fully considered. Many scaling laws followed the work of Mattax and Kyte (1962). For instance, the subsequent relation developed by Ma et al. (1997) was of significance as it integrated a new characteristic length in the scaling law that accounts for different boundary conditions, resulting in the development of a semi-empirical relationship. However, the scaling law is valid in strongly waterwet systems exclusively. Recently, Schmid and Geiger (2012) developed a new scaling law based on the semi-analytical solutions of McWhorter and Sunada (1990, 1992) presented earlier in this paper, thus relaxing the conditions under which the scaling law is valid. However, this relation fails to predict the shape of the final recovery over the whole range of time, but rather valid until:

$$t^* = \left[\frac{L_c\phi}{2CF'(S_{wir})}\right]^2 \tag{44}$$

The analytical solution predicts an indefinite increase in the cumulative volume of water imbibed Q_w as time becomes infinite. However, this early time solution is only valid until the wetting front reaches the end of the matrix block (i.e. the water flow is affected by no-flow boundary conditions). Hence, an exponential model can be used to predict the recovery over the entire time range. This function is based on approximate analytical solutions that is used to derive an improved transfer rate. However, the exponential model is pessimistic in the prediction of early time recovery, which as shown previously, scales at the square-root of time Schmid and Geiger (2012). The fitted model is as follows:

$$R = R_\infty\left(1 - e^{-\alpha t_D}\right) \tag{45}$$

where t_D is:

$$t_D = \left[\frac{Q_w(t)}{\phi L_c}\right]^2 = \left[\frac{2C}{\phi L_c}\right]^2 t \tag{46}$$

and $\alpha \approx 70$. This empirical value is obtained experimentally and is independent of wettability states and rock material.

This scaling law is considered the master equation for fitting spontaneous imbibition data in both water-wet and mixed-wet systems. To prove the superiority of the scaling group over the previously developed laws, Schmid and Geiger (2012) tested the results of scaling the oil recovery analytically against 45 published experimental results with different wettability conditions, viscosity ratios and boundary conditions (Hamon and Vidal, 1986; Bourbiaux and Kalaydjian, 1990; Zhang et al., 1996; Zhou et al., 2002; Fischer et al., 2006; Hatiboglu and Babadagli, 2007; Babadagli and Hatiboglu, 2007; Mason and Morrow, 2013). The scaling group showed a good agreement with the experimental results, in the sense that the experimental results fell on one universal curve, thus proving its validity for a wide range of data. Fig. 13 shows the work of Schmid and Geiger in comparing their scaling group with the Ma et al. (1997) model. The dimensionless time of Ma et al. (1997) is derived based on the characteristic length, *L* and depends on an empirical factor that is easily measured; the square root of the product of the viscosities of the wetting and the non-wetting phases. The model can be represented as:

$$t_D = \frac{1}{L_c}\sqrt{\frac{k}{\phi}}\frac{\sigma}{\sqrt{\mu_w\mu_{nw}}} \tag{47}$$

where μ_w and μ_{nw} represented the viscosity of the wetting and the non-wetting phase respectively.

The data in Fig. 13 does not collapse into one curve for Ma et al. (1997) on the contrary to the universal scaling group by Schmid and Geiger (2012) where the data falls neatly into a narrow range.

In Abd and Alyafei (2018), the applicability of the Schmid and Geiger (2012) scaling group was also tested. For this purpose, 16

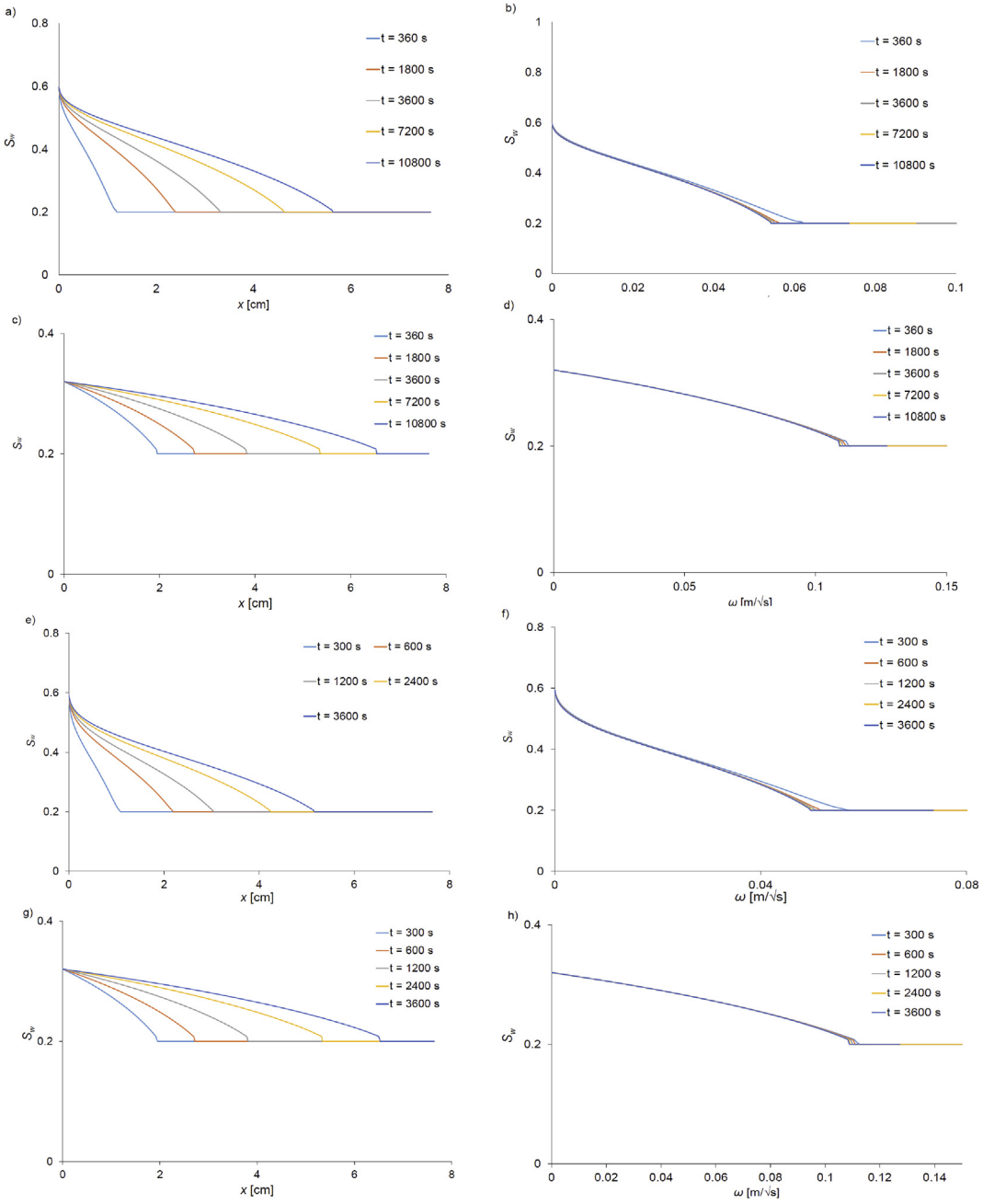

Fig. 10. Water saturation profiles plotted against time and scaled time: (a) and (b) are strongly water-wet cases with M = 1; (c) and (d) are mixed-wet with M = 1; (e) and (f) are strongly water-wet with M = 3; (g) and (h) are mixed-wet with M = 3.

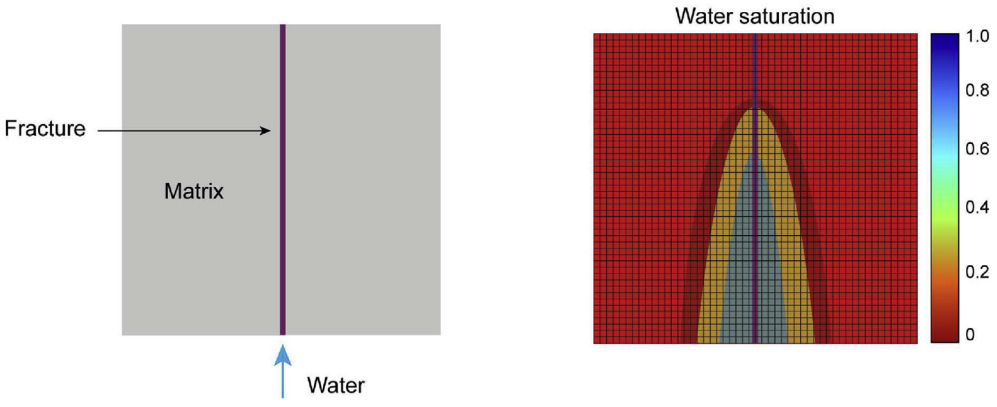

Fig. 11. The fracture connecting an injector and a producer is shown (left). The oil is displaced due to spontaneous imbibition into the fracture which is then moved up to the producer by the water flow from the injector. This process is shown on a simulation grid depicting the change in the saturation profile along the fracture (right). Reproduced from Andersen et al. (2014).

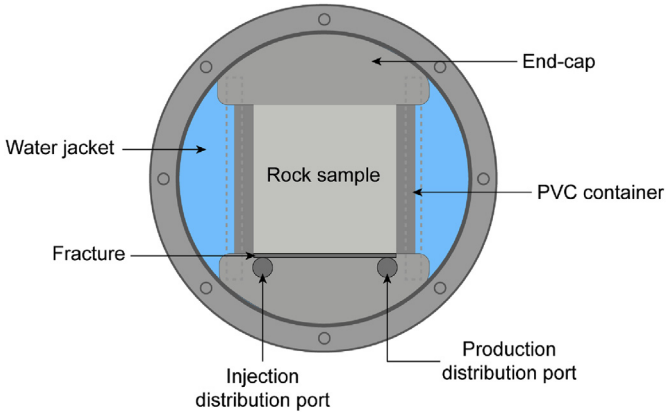

Fig. 12. The frontal view of a core holder of cubic rock samples. Reproduced from Rangel-German and Kovscek (2006).

synthetic data sets with varying boundary conditions were generated, with different characteristic lengths, porosity, permeability, viscosity and rock parameters. The samples were divided into two main parts, where the "S" sample mimics the behavior of Schmid et al. (2016) data and the "B" sample are based on the data sets provided by Blunt (2017). The different samples are summarized in Table 3 below.

Upon simulating the 16 cases, the numerical results were used to calculate the dimensionless time of the two tested groups, and the ultimate recovery curves were plotted on a semi-logarithmic scale in Fig. 14. The semi-analytical solution was used to calculate the *C* values for each case, which in turn are used to derive the dimensionless time. It is noticed that Ma et al. (1997) group was less effective in scaling all of the data sets, as opposed to the universal scaling group by Schmid and Geiger (2012). The variations in the rock and fluid properties did not affect the quality of scaling for the latest group, as the data falls into one single curve without significant scatter. Moreover, numerical modelling allows us to predict the recovery curves even at late times when the water front reaches to a boundary condition. The topic of upscaling different sets of data, and the impact of the different controlling parameters on the quality of the scaling are studied in detail by Abd and Alyafei (2018) which can be referred to for further details.

3.4. Applications of the semi-analytical solution

The semi-analytical solution for SI can be used to estimate the relative permeabilities and capillary pressure from SI experimental results (Li and Horne, 2005; Khan and Alyafei, 2017; Alyafei and Blunt, 2018). We can match the measured saturation profiles to the semi-analytical solutions by manipulating the parameters related to the relative

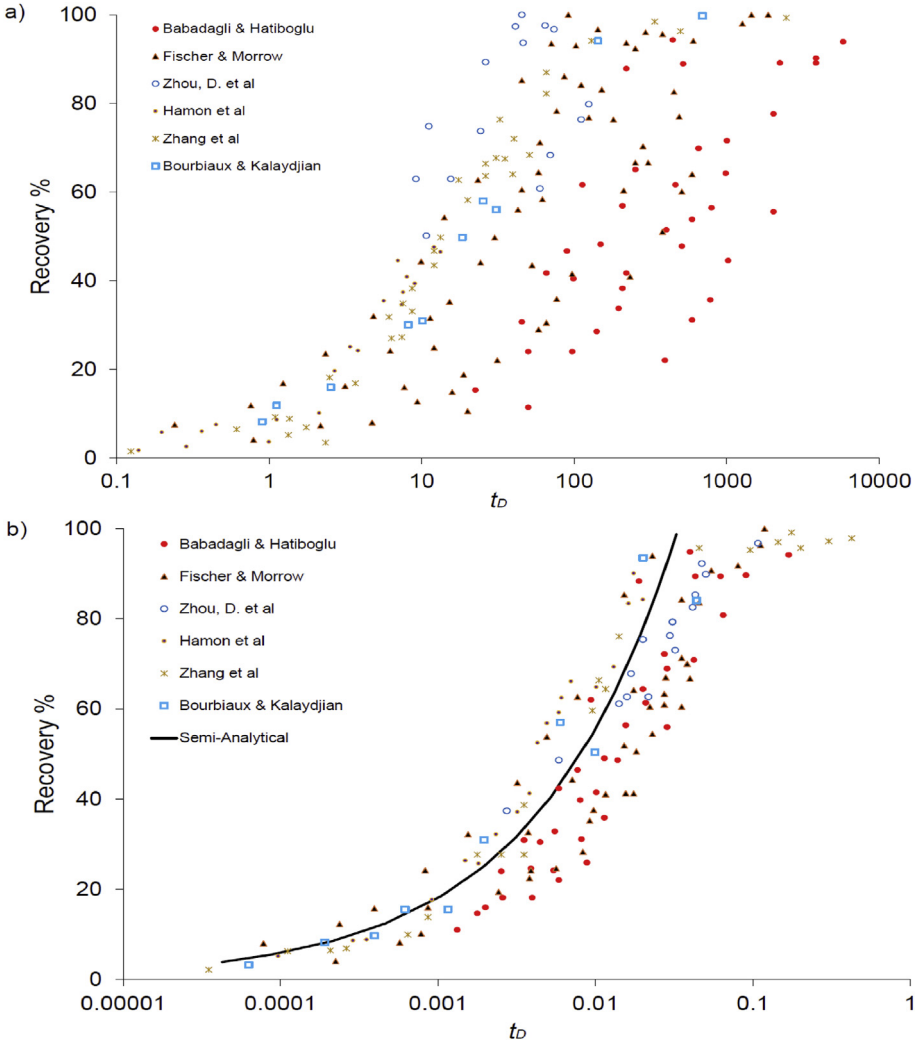

Fig. 13. Oil recovery versus time, where (a) The Ma et al. (1997) scaling group, equation (56), is used to scale the experimental data but effective wide scatter in the data is still evident. (b) The Schmid and Geiger (2012) scaling group, equation (54–55) is used and the data falls onto a curve with little scatter, independent of the material or fluid characteristics. Reproduced from Schmid and Geiger (2012).

Table 3
The rock and fluid parameters used to synthesize the data sets for numerical modelling of SWW rock, where each sample represent the parameters used to generate an oil recovery curve (BC in the table stands for boundary condition). From Abd and Alyafei (2018).

Sample	BC	L_c [cm]	k [mD]	k [m^2]	ϕ	μ_w [mPa.s]	μ_{nw} [mPa.s]	S_w	S_o	k_{rw}	k_{ro}
S1	OEO	7.66	300	2.96×10^{-13}	0.2	1	3	0.2	0.4	0.2	0.85
S2	TEO	3.83	300	2.96×10^{-13}	0.2	1	3	0.2	0.4	0.2	0.85
S3	TEC	2.71	300	2.96×10^{-13}	0.2	1	3	0.2	0.4	0.2	0.85
S4	AFO	0.86	300	2.96×10^{-13}	0.2	1	3	0.2	0.4	0.2	0.85
S5	TEO	3.83	300	2.96×10^{-13}	0.25	1	3	0.2	0.4	0.2	0.85
S6	TEO	3.83	300	2.96×10^{-13}	0.2	1	1	0.2	0.4	0.2	0.85
S7	TEO	3.83	300	2.96×10^{-13}	0.2	1	10	0.2	0.4	0.2	0.85
S8	TEC	2.71	500	4.93×10^{-13}	0.2	1	3	0.2	0.4	0.3	0.85
B1	TEC	2.71	300	2.96×10^{-13}	0.2	1	3	0.2	0.4	0.1	0.85
B2	TEO	2.71	300	2.96×10^{-13}	0.2	1	3	0.2	0.4	0.05	0.85
B3	AFO	0.86	300	2.96×10^{-13}	0.2	1	3	0.1	0.4	0.2	0.85
B4	AFO	0.86	250	2.47×10^{-13}	0.2	1	3	0.4	0.4	0.2	0.85
B5	AFO	0.86	300	2.96×10^{-13}	0.2	1	3	0.0	0.4	0.2	0.85
B6	OEO	7.66	1000	9.87×10^{-13}	0.25	1	20	0.1	0.4	0.1	1
B7	TEO	3.83	1000	9.87×10^{-13}	0.25	1	3	0.1	0.2	0.1	1
B8	TEC	2.71	1000	9.87×10^{-13}	0.25	1	200	0.1	0.2	0.1	1

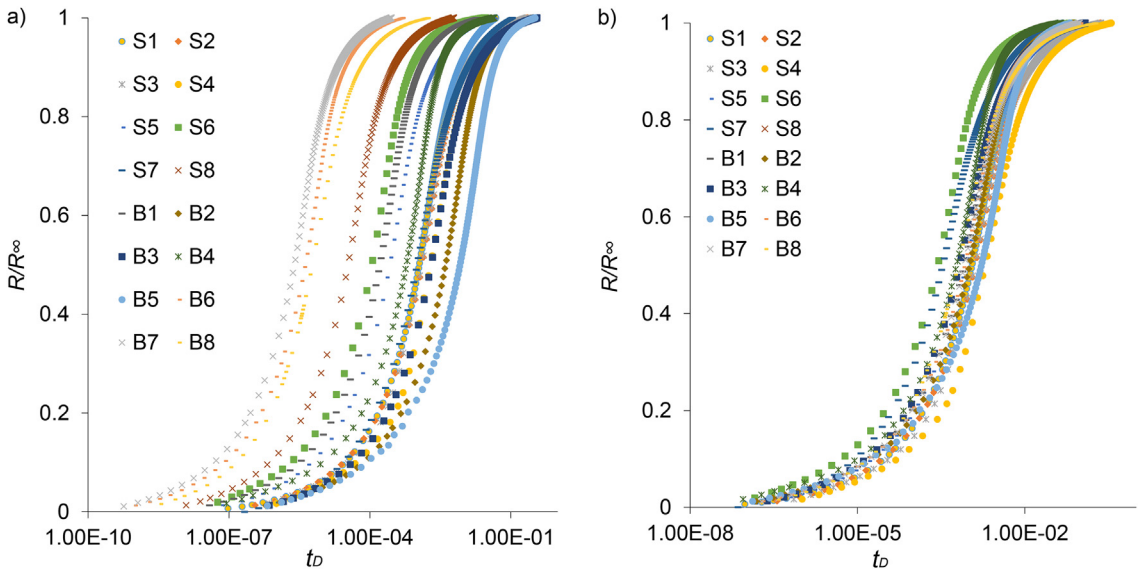

Fig. 14. The oil recovery as a function of dimensionless time for different scaling groups: (a) Ma et al. (1997), equation (55), does not scale the different data sets and fail to converge the result into one single curve (b) Schmid and Geiger (2012), equations (54–55), scales the 16 different data sets into one single curve validating its universal applicability. Reproduced from Abd and Alyafei (2018).

permeabilities and capillary pressure. Since the spontaneous imbibition profile depends on hydrocarbon and water relative permeabilities, and capillary pressure, the experimental measurements alone are not enough to determine all three functions. However, if the relative permeabilities could be determined experimentally, then a comparison with the semi-analytical solution would be enough to determine the capillary pressure. In brief, the semi-analytical solution complements traditional core measurements in determining the flow properties.

An experimental water saturation profile was extracted from a study on a diatomite core, where CT-measured saturation images were presented (Le Guen and Kovscek, 2006). The core was initially saturated with decane, with no initial water present. The water progressed uniformly through the core in a one-dimensional profile. The water saturation averaged perpendicular to the average flow direction is shown, as a function of distance from the inlet at different times, in Fig. 15. After obtaining the experimental profile, the results were matched with the semi-analytical solutions. However, no information on the relative permeabilities and the capillary pressure was provided, and thus the estimation in not unique, but rather one possible interpretation of the situation. The process was started the process by adjusting the parameters shown in Table 4, while using the provided porosity, viscosity, permeability and core length from the experimental dataset. We manipulated the parameters and iterated on the constant C until a profile match was obtained. The matched parameters are tabulated in Table 4. The parameters are then used to run a simulation case and obtain numerical water saturation profiles. The numerical simulations were added as a checkpoint, to make sure that the results of the semi-analytical solution can be replicated using the simulation code. The three curves representing the experimental, semi-analytical and numerical data are plotted in Fig. 15 against the scaled time. We notice clearly that the experimental data scales as the square root of time, as the three saturation curves fall into one unified profile. Moreover, the fitted semi-analytical solution matches the general trend of the measured data with the experimental profiles scattered around the mathematical solution. Based on the match quality, we could confidently say that the parameters obtained in Table 4 form a plausible set of rock properties for the experiment presented. Hence, the semi-analytical solution of SI could be used to estimate the relative permeability and capillary pressure of a rock through matching the experimental and semi-analytical water saturation profiles. This routine is advantageous as it substitutes the costly core analysis tests with an easier approach without a great effect on the accuracy of the parameters. Moreover, by construction,

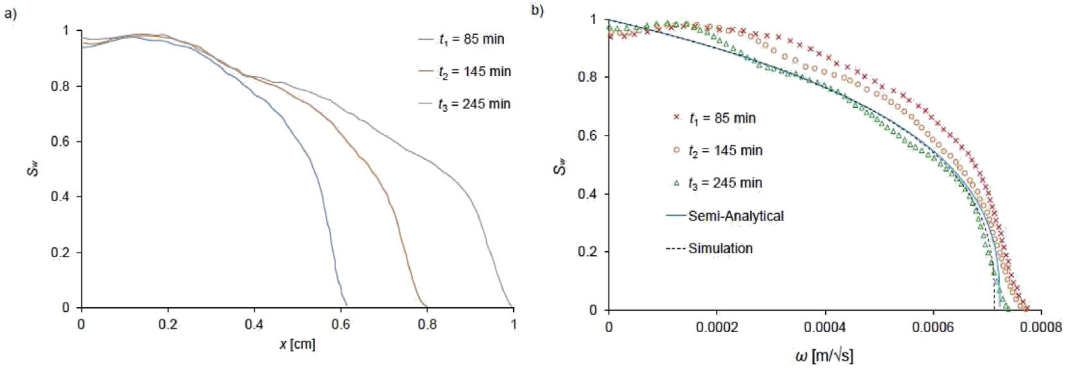

Fig. 15. (a) The experimental water saturation profiles are plotted against core distance and different times. (b) The experimental water saturation profiles scale with the square root of time to form a single curve. The fitted semi-analytical solution and the simulated numerical profile are plotted, and they match well with the experimental data. Experimental data from Le Guen and Kovscek (2006).

Table 4
The parameters obtained from fitting the semi-analytical solution against the experimental data.

Parameter	Fitted value
S_{wir}	0
S_{or}	0
$k_{rw\ max}$	0.1
n	3
$k_{ro\ max}$	1
m	1
P_{entry} $[kPa]$	12000
P_a $[kPa]$	2500
l	0.254
μ_w $[mPa.\ s]$	1
μ_{nw} $[mPa.\ s]$	0.018
$C_{counter\text{-}current}$ $[m/\sqrt{s}]$	1.76×10^{-6}

this method correctly compute the imbibition rate which is useful for application in dual porosity reservoir simulation where imbibition is the dominant recovery process.

4. Conclusions and future work

Counter-current spontaneous imbibition is an important phenomenon during secondary production of fractured reservoirs. Numerous works have characterized and modelled this phenomenon with analytical and numerical approaches. Successful estimation of counter-current SI rates is of great significance when it comes to conventional field predictions.

The experimental works of Dong and Zhou (1998) and Unsal et al. (2009) on SI processes have proved to be important as they portray the closest scenarios to capillaries in pore systems with fluid exchange based on differences in phase pressures, and hence the occurrence of counter-current spontaneous imbibition. Their works provided physical insight into the displacement mechanisms that occur during SI, combined with analytical expressions of the advance of the wetting phase. On the other hand, the semi-analytical solution of Schmid et al. (2011) is a very important tool to estimate oil recovery from naturally fractured reservoirs. The semi-analytical solution helps to evaluate the capillary pressure and relative permeability and provides predictions of fluid flow in the reservoir. Subsequent research has verified the validity of the solution and suggested it as a replacement to routine core analysis experiments to obtain different rock parameters. Here, we presented a simplified theoretical treatment and a straightforward way to construct solutions.

Based on the semi-analytical solution of Schmid et al. (2011), a master scaling transfer function for SI in oil recovery has been developed. The scaling law of Schmid and Geiger (2012) upscales laboratory results to the field scale for both water-wet and mixed-wet systems. The scaling group is valid for a wide range of different rocks and fluid properties. Furthermore, unlike previously developed expressions, there are only few limiting constraints. The scaled water saturation profiles can be used to predict oil flow in reservoirs with better confidence and reliability than the more empirical approaches used previously.

Future work could consider the analysis of SI in transition zone reservoirs where the wettability varies with height above the free water level (Marion et al., 2003). Experimentally, the *in situ* monitoring of the SI saturation profile, combined with traditional core analysis measurements could be used to determine or constrain relative permeability and capillary pressure. Of particular interest is the use of saturation monitoring to find the water relative permeability in mixed-wet systems at low water saturation: its low value limits the rate of SI, allowing careful and accurate determination of the evolution of the profile in a SI experiment, which is otherwise difficult to measure using traditional steady-state or unsteady-state relative permeability tests.

The core scale work done up to this point proved very useful scientifically for testing different scaling groups and understanding how backpressure and oil recovery can be properly predicted and upscaled using core data. Due to rock properties changing laterally and not allowing a single core's properties to be applicable throughout a reservoir, possible future work can address a method to upscale to the full field scale in heterogeneous reservoirs using results from several core samples.

Acknowledgments

We would like to acknowledge Qatar National Research Fund, QNRF, project number NPRP10-0101-170086 for funding this project.

Nomenclature

δ_{Ai}	distance from the open surface to the center of the matrix block [m]
λ_t	total mobility [1/Pa.s]
λ_w	wetting phase mobility [1/Pa.s]
λ_{nw}	non-wetting mobility [1/Pa.s]
μ	viscosity [Pa.s]
μ_d	viscosity of displaced fluid [Pa.s]
μ_{nw}	viscosity of the non-wetting phase [Pa.s]
μ_w	viscosity of the wetting phase [Pa.s]
ρ_{nw}	density of the non-wetting phase [kg/m^3]
ρ_w	density of the wetting phase [kg/m^3]
σ	interfacial tension [N/m]
ϕ	porosity
ω	scaling factor [m/√s]

A_i	surface open to imbibition in the i-th direction [m^2]
A_t	actual value
C	imbibition constant [m/√s]
D	capillary dispersion coefficient [m^2/s]
F	capillary dominated fractional flow
F'	first derivative of F
F''	second derivative of F
F_s	shape factor
F_t	forecast value
f	Buckley-Leverett fractional flow
k	permeability [m^2]
k_{rw}	water relative permeability
k_{ro}	oil relative permeability
$k_{rw\ max}$	maximum water relative permeability
$k_{ro\ max}$	maximum oil relative permeability
L	total length of capillary tube [m]
L_{max}	maximum length of the core
l	capillary pressure exponent
M	viscosity ratio
m	non-wetting phase Corey exponent
n	wetting phase Corey exponent
n_i	total number of data points
P_c	capillary pressure [Pa]
dP_c/dx	capillary pressure gradient [Pa/m]
P_{cb}	capillary back pressure [Pa]
P_{dead}	dead-end pressure created at the interface between capillaries [Pa]
P_{entry}	entry capillary pressure [Pa]
P_f	fracture capillary pressure [Pa]
P_m	matrix capillary pressure [Pa]
ΔP	pressure drop across an axial length x [Pa]
Q_w	cumulative volume of water imbibed [m^3]
q_{nw}	non-wetting phase velocity [m/s]
q_o	oil Darcy velocity [m/s]
q_t	total velocity [m/s]
q_w	water Darcy velocity [m/s]
RF	recovery factor
r	radius [m]
S_{xo}	saturation at the inlet
S_w	water saturation
S_w^*	water saturation when capillary pressure is zero
S_o	oil saturation
S_{or}	residual oil saturation
S_{wi}	initial water saturation
S_{wir}	irreducible water saturation
t	time [s]
t_D	dimensionless time
V_b	bulk volume of matrix block [m^3]
υ	mean velocity [m/s]
x	distance in the core [m]

References

Abd, A., Alyafei, N., 2018. Numerical investigation on the effect of boundary conditions on the scaling of spontaneous imbibition. Oil Gas Sci. Technol. Revue D'IFP Energies Nouvelles 73, 71.

Abushaikha, A., Gosselin, O., 2008. Matrix-fracture transfer function in dual-media flow simulation: review, comparison and validation. In: Proceedings of the Europec/EAGE Conference and Exhibition.

Akin, S., Schembre, J., Bhat, S., Kovscek, A., 2000. Spontaneous imbibition characteristics of diatomite. J. Pet. Sci. Eng. 25 (3–4), 149–165.

Al-Hadhrami, H., Blunt, M., 2001. Thermally induced wettability alteration to improve oil recovery in fractured reservoirs. SPE Reservoir Eval. Eng. 4 (03), 179–186.

Alyafei, N., Al-Menhali, A., Blunt, M., 2016. Experimental and analytical investigation of spontaneous imbibition in water-wet carbonates. Transport Porous Media 115 (1), 189–207.

Alyafei, N., Blunt, M., 2018. Estimation of relative permeability and capillary pressure from mass imbibition experiments. Adv. Water Resour. 115, 88–94.

Alyafei, N., Solling, T., Blunt, M., 2014. Investigation of co-current and counter-current spontaneous imbibition using micro-computerized tomography. In: Proceedings of the International Symposium of the Society of Core Analysis, SCA2014-098.

Andersen, P.Ø., Brattekås, B., Walrond, K., Aisyah, D.S., Nødland, O., Lohne, A., Fernø, M., 2017. Numerical interpretation of laboratory spontaneous imbibition-incorporation of the capillary back pressure and how it affects SCAL. In: Proceeding of the Abu Dhabi International Petroleum Exhibition & Conference.

Andersen, P., Evje, S., Kleppe, H., 2014. A model for spontaneous imbibition as a mechanism for oil recovery in fractured reservoirs. Transport Porous Media 101 (2), 299–331.

Anderson, W., 1986. Wettability literature survey-part 2: wettability measurement. J. Pet. Technol. 38 (11) 1, 246-241.

Arabjamaloei, R., Shadizadeh, S., 2010. A new approach for specifying imbibition face boundary condition in countercurrent spontaneous imbibition. Petrol. Sci. Technol. 28 (18), 1855–1862.

Babadagli, T., Ershaghi, I., 1992. Imbibition assisted two-phase flow in natural fractures. In: Proceedings of the SPE Western Regional Meeting, SPE 24044.

Babadagli, T., Hatiboglu, C., 2007. Analysis of counter-current gas–water capillary imbibition transfer at different temperatures. J. Pet. Sci. Eng. 55 (3–4), 277–293.

Barenblatt, G., Entov, V., Ryzhik, V., 1990. Theory of Fluid Flows through Natural Rocks. Springer.

Barenblatt, G., Patzek, T., Silin, D., 2003. The mathematical model of nonequilibrium effects in water-oil displacement. SPE J. 8 (04), 409–416.

Barenblatt, G., Zheltov, I., Kochina, I., 1960. Basic concepts in the theory of seepage of homogeneous liquids in fissured rocks. J. Appl. Math. Mech. 24 (5), 1286–1303.

Bartley, J., Ruth, D., 1999. Relative permeability analysis of tube bundle models. Transport Porous Media 36 (2), 161–188.

Behbahani, H.S., Di Donato, G., Blunt, M., 2006. Simulation of counter-current imbibition in water-wet fractured reservoirs. J. Pet. Sci. Eng. 50 (1), 21–39.

Behbahani, H., Blunt, M., 2005. Analysis of imbibition in mixed-wet rocks using pore-scale modeling. Soc. Petrol. Eng. J. 10 (04), 466–474.

Bell, J., Cameron, F., 1906. The flow of liquids through capillary spaces. J. Phys. Chem. 10 (8), 658–674.

Bjørnarå, T., Mathias, S., 2013. A pseudospectral approach to the McWhorter and Sunada equation for two-phase flow in porous media with capillary pressure. Comput. Geosci. 17 (6), 889–897.

Blunt, M., 2017. Multiphase Flow in Permeable Media: A Pore-Scale Perspective. Cambridge University Press.

Bourbiaux, B., Kalaydjian, F., 1990. Experimental study of co-current and countercurrent flows in natural porous media. SPE Reservoir Eng. 5 (03), 361–368.

Canale, R., Chapra, S., 1998. Numerical Methods for Engineers with Programming and Software Applications, third ed. McGraw-Hill.

Chen, J., Miller, M., Sepehrnoori, K., 1995. Investigations of matrix-fracture transfer flows in dual porosity modeling of naturally fractured reservoirs. In: Proceedings of the Low Permeability Reservoirs Symposium.

Cil, M., Reis, J., 1996. A multi-dimensional, analytical model for counter-current water imbibition into gas-saturated matrix blocks. J. Pet. Sci. Eng. 16 (1–3), 61–69.

Cil, M., Reis, J., Miller, M., Misra, D., 1998. An examination of countercurrent capillary imbibition recovery from single matrix blocks and recovery predictions by analytical matrix/fracture transfer functions. In: SPE Annual Technical Conference and Exhibition.

Cuiec, L., Bourbiaux, B., Kalaydjian, F., 1994. Oil recovery by imbibition in low-permeability chalk. SPE Form. Eval. 9 (3), 200–208.

Dake, L., 1983. Fundamentals of Reservoir Engineering. Elsevier.

Dong, M., Dullien, F., 1997. A new model for immiscible displacement in porous media. Transport Porous Media 27 (2), 185–204.

Dong, M., Dullien, F.A.L., Zhou, J., 1998. Characterization of waterflood saturation profile histories by the 'complete' capillary number. Transp. Porous Media 31 (2), 213–237. https://doi.org/10.1023/A:1006565621860.

Dong, M., Dullien, F., Dai, L., Li, D., 2005. Immiscible displacement in the interacting capillary bundle model part I. Development of interacting capillary bundle model. Transport Porous Media 59 (1), 1–18.

Dong, M., Zhou, J., 1998. Characterization of waterflood saturation profile histories by the 'complete' capillary number. Transport Porous Media 31 (2), 213–237.

Fischer, H., Wo, S., Morrow, N., 2006. Modeling the effect of viscosity ratio on spontaneous imbibition. SPE Reservoir Eval. Eng. 102641, 577–589.

Fokas, A., Yortsos, Y., 1982. On the exactly solvable equation S_t = (βS + γ)^-2S_x_x + α(βS + γ)^-2S_x occurring in two-phase flow in porous media. SIAM J. Appl. Math. 42 (2), 318–332.

Foley, A., Nooruddin, H., Blunt, M., 2017. The impact of capillary backpressure on spontaneous counter-current imbibition in porous media. Adv. Water Resour. 107, 405–420.

Garg, A., Kovscek, A., Nikrakvesh, M., Castanier, L., Patzek, T., 1996. CT scan and neural network technology for construction of detailed distribution of residual oil saturation during waterflooding. In: Proceedings of the Western Regional Meeting, SPE 35737.

Gilman, J., Kazemi, H., 1983. Improvements in simulation of naturally fractured reservoirs. Soc. Petrol. Eng. J. 23 (04), 695–707.

Gong, J., Rossen, W., 2018. Characteristic fracture spacing in primary and secondary recovery for naturally fractured reservoirs. Fuel 223, 470–485.

Hamon, G., Vidal, J., 1986. Scaling-up the capillary imbibition process from laboratory experiments on homogeneous samples. In: Proceedings of the SPE European Petroleum Conference, SPE 15852.

Handy, L., 1960. Determination of effective capillary pressure for porous media from imbibition data. Soc. Petrol. Eng. 219, 75–80.

Hatiboglu, C., Babadagli, T., 2007. Oil recovery by counter-current spontaneous imbibition: effects of matrix shape factor, gravity, IFT, oil viscosity, wettability, and rock type. J. Pet. Sci. Eng. 59 (1–2), 106–122.

Hatiboglu, C., Babadagli, T., 2008. Pore-scale studies of spontaneous imbibition into oil-saturated porous media. Phys. Rev. 77 (6), 066311.
Haugen, Å., Fernø, M., Mason, G., Morrow, N., 2014. Capillary pressure and relative permeability estimated from a single spontaneous imbibition test. J. Pet. Sci. Eng. 115, 66–77.
Helmig, R., 1997. Multiphase Flow and Transport Processes in the Subsurface: a Contribution to the Modeling of Hydrosystems. Springer-Verlag.
Iffly, R., Rousselet, D., Vermeulen, J., 1972. Fundamental study of imbibition in fissured oil fields. In: Proceedings of the Society of Petroleum Engineers of AIME Fall Meeting.
Kashchiev, D., Firoozabadi, A., 2003. Induction time in crystallization of gas hydrates. J. Cryst. Growth 250 (3–4), 499–515.
Kazemi, H., Gilman, J., Elsharkawy, A., 1992. Analytical and numerical solution of oil recovery from fractured reservoirs with empirical transfer functions (includes associated papers 25528 and 25818). SPE Reservoir Eng. 7 (02), 219–227.
Kazemi, H., Merrill, L., Porterfield, K., Zeman, P., 1976. Numerical simulation of water-oil flow in naturally fractured reservoirs. Soc. Petrol. Eng. J. 16 (06), 317–326 SPE 5719.
Khan, A., Alyafei, N., 2017. Investigation of an analytical solution for spontaneous imbibition to effectively estimate special core analysis SCAL properties. In: Proceedings of the SPE Annual Caspian Technical Conference and Exhibition.
Khan, A., Siddiqui, A., Abd, A., Alyafei, N., 2018. Guidelines for numerically modeling Co-and counter-current spontaneous imbibition. Transport Porous Media 124 (3), 743–766.
Kleppe, J., Morse, R., 1974. Oil production from fractured reservoirs by water displacement. In: Proceedings of the Society of Petroleum Engineers Fall Meeting.
Le Guen, S., Kovscek, A., 2006. Nonequilibrium effects during spontaneous imbibition. Transport Porous Media 63 (1), 127–146.
Li, C., Shen, Y., Ge, H., Zhang, Y., Liu, T., 2018. Spontaneous imbibition in fractal tortuous micro-nano pores considering dynamic contact angle and slip effect: phase portrait analysis and analytical solutions. Sci. Rep. 8 (1), 3919.
Li, K., Horne, R., 2000. Characterization of spontaneous imbibition into gas-saturated rocks. In: Proceedings of the SPE/AAPG Western Regional Meeting, SPE62552.
Li, K., Horne, R., 2005. Extracting capillary pressure and global mobility from spontaneous imbibition data in oil-water-rock systems. Soc. Petrol. Eng. J. 10 (04), 458–465.
Lu, H., Blunt, M., 2007. General fracture/matrix transfer functions for mixed-wet systems. In: Proceedings of the EUROPEC/EAGE Conference and Exhibition.
Lucas, R., 1918. Ueber das Zeitgesetz des kapillaren Aufstiegs von Flüssigkeiten. Colloid Polym. Sci. 23 (1), 15–22.
Ma, S., Morrow, N.R., Zhang, X., 1997. Generalized scaling of spontaneous imbibition data for strongly water-wet systems. J. Pet. Sci. Eng. 18 (3-4), 165–178.
Marion, D., Noman, R., Al-Othman, I., Leschi, P., 2003. The development of Al Khalij-a complex carbonate field, offshore Qatar. Soc. Pet. Eng. https://doi.org/10.2118/81574-MS.
Mason, G., Fischer, H., Morrow, N., Ruth, D., 2009. Spontaneous counter-current imbibition into core samples with all faces open. Transport Porous Media 78 (2), 199–216.
Mason, G., Morrow, N., 2013. Developments in spontaneous imbibition and possibilities for future work. J. Pet. Sci. Eng. 110, 268–293.
Mattax, C., Kyte, J., 1962. Imbibition oil recovery from fractured, water-drive reservoir. Soc. Petrol. Eng. J. 2 (02), 177–184.
McWhorter, D., Sunada, D., 1992. Reply [to “comment on ‘exact integral solutions for two-phase flow’ by David B. McWhorter and Daniel K. Sunada”]. Resour. Res. 28 (5) 1479-1479.
McWhorter, D., Sunada, D., 1990. Exact integral solutions for two-phase flow. Water Resour. Res. 26 (3), 399–413.
Meng, Q., Liu, H., Wang, J., 2017a. A critical review on fundamental mechanisms of spontaneous imbibition and the impact of boundary condition, fluid viscosity and wettability. Adv. Geo-Energy Res. 1 (1), 1–17.
Meng, Q., Liu, H., Wang, J., Liu, H., 2017b. Effect of fluid viscosity on correlation of oil recovery by linear counter-current spontaneous imbibition. J. Pet. Sci. Eng. 151, 341–347.
Mirzaei-Paiaman, A., Kord, S., Hamidpour, E., Mohammadzadeh, O., 2017. Scaling one- and multi-dimensional co-current spontaneous imbibition processes in fractured reservoirs. Fuel 196, 458–472.
Morrow, N., Mason, G., 2001. Recovery of oil by spontaneous imbibition. Curr. Opin. Colloid Interface Sci. 6 (4), 321–337.
Muggeridge, A., Cockin, A., Webb, K., Frampton, H., Collins, I., Moulds, T., Salino, P., Sciences, E., 2014. Recovery rates, enhanced oil recovery and technological limits. Phil. Trans. Math. Phys. Eng. Sci. 372 (2006), 20120320.
Nooruddin, H., Blunt, M., 2016. Analytical and numerical investigations of spontaneous imbibition in porous media. Water Resour. Res. 52 (9), 7284–7310.
Olafuyi, O., Cinar, Y., Knackstedt, M., Pinczewski, W., 2007. Spontaneous imbibition in small cores. In: Proceedings of the in Asia Pacific Oil and Gas Conference.
Prey, D., Lefebvre, E., 1978. Gravity and capillarity effects on imbibition in porous media. Soc. Petrol. Eng. J. 18 (03), 195–206.
Qasem, F., Nashawi, I., Gharbi, R., Mir, M., 2008. Recovery performance of partially fractured reservoirs by capillary imbibition. J. Pet. Sci. Eng. 60 (1), 39–50.
Quandalle, P., Sabathier, J., 1989. Typical features of a multipurpose reservoir simulator. SPE Reservoir Eng. 4 (04), 475–480.
Rangel-German, E., Kovscek, A., 2002. Experimental and analytical study of multi-dimensional imbibition in fractured porous media. J. Pet. Sci. Eng. 36 (1–2), 45–60.
Rangel-German, E., Kovscek, A., 2006. Time-dependent matrix-fracture shape factors for partially and completely immersed fractures. J. Pet. Sci. Eng. 54 (3–4), 149–163.
Rapoport, 1955. Scaling laws for use in design and operation of water-oil flow models. Trans. AIME 204, 143–150.
Reis, J., Cil, M.J.I.S., 1999. Analytical models for capillary imbibition: one-dimensional matrix blocks. Situ 23 (3), 243–270.
Ruth, D., Bartley, J., 2011. Capillary tube models with interaction between the tubes. Transport Porous Media 86 (2), 479–482.
Ruth, D., Arthur, J., 2011. A revised analytic solution to the linear displacement problem including capillary pressure effects. Transport Porous Media 86 (3), 881–894.
Saidi, A., 1983. Simulation of naturally fractured reservoirs. In: SPE Reservoir Simulation Symposium.
Salimi, H., Bruining, J., 2010. Improved prediction of oil recovery from waterflooded fractured reservoirs using homogenization. SPE Reservoir Eval. Eng. 13 (01), 44–55.
Schlumberger, 2013. Carbonate Reservoirs. http://www.slb.com/services/technical_challenges/carbonates.aspx.
Schmid, K.S., Alyafei, N., Geiger, S., Blunt, M., 2016. Analytical solutions for spontaneous imbibition: fractional-flow theory and experimental analysis. Soc. Petrol. Eng. J. 21 (06) 2,308-302,316.
Schmid, K., Geiger, S., 2012. Universal scaling of spontaneous imbibition for water-wet systems. Water Resour. Res. 48 (3).
Schmid, K., Geiger, S., 2013. Universal scaling of spontaneous imbibition for arbitrary petrophysical properties: water-wet and mixed-wet states and Handy's conjecture. J. Pet. Sci. Eng. 101, 44–61.
Schmid, K., Geiger, S., Sorbie, K., 2011. Semianalytical solutions for co-current and countercurrent imbibition and dispersion of solutes in immiscible two-phase flow. Water Resour. Res. 47 (2).
Thomas, L., Dixon, T., Pierson, R., 1983. Fractured reservoir simulation. Soc. Petrol. Eng. J. 23 (01), 42–54.
Unsal, E., Mason, G., Morrow, N., Ruth, D., 2007a. Co-current and counter-current imbibition in independent tubes of non-axisymmetric geometry. J. Colloid Interface Sci. 306 (1), 105–117.
Unsal, E., Mason, G., Morrow, N., Ruth, D., 2009. Bubble snap-off and capillary-back pressure during counter-current spontaneous imbibition into model pores. Langmuir 25 (6), 3387–3395.
Unsal, E., Mason, G., Ruth, D., Morrow, N., 2007b. Co-and counter-current spontaneous imbibition into groups of capillary tubes with lateral connections permitting cross-flow. J. Colloid Interface Sci. 315 (1), 200–209.
Warren, J., Root, P., 1963. The behavior of naturally fractured reservoirs. Soc. Petrol. Eng. J. 3 (03), 245–255.
Washburn, E., 1921. The dynamics of capillary flow. Phys. Rev. 17 (3), 273–283.
Yu, L., Evje, S., Kleppe, H., Kårstad, T., Fjelde, I., Skjaeveland, S., 2009. Spontaneous imbibition of seawater into preferentially oil-wet chalk cores—experiments and simulations. J. Pet. Sci. Eng. 66 (3–4), 171–179.
Zhang, X., Morrow, N., Ma, S., 1996. Experimental verification of a modified scaling group for spontaneous imbibition. SPE Reservoir Eng. 11 (04), 280–285.
Zhou, D., Jia, L., Kamath, J., Kovscek, A., 2002. Scaling of counter-current imbibition processes in low-permeability porous media. J. Pet. Sci. Eng. 33 (1–3), 61–74.